Journal of Process Control 81 (2019) 136–149

Contents lists available at ScienceDirect

Journal of Process Control

journal homepage: www.elsevier.com/locate/jprocont

Data-driven modeling and optimal control of the production of Fructo-Oligosaccharides by *Aureobasidium Pullulans*

R. Fekih-Salem[a,c], J. Schorsch[d], L. Dewasme[a,*], C. Castro[b], A.-L. Hantson[b], M. Kinnaert[d], A. Vande Wouwer[a]

[a] *Automatic Control Laboratory, Faculty of Engineering, University of Mons, 7000 Mons, Belgium*
[b] *Chemical and Biochemical Process Engineering Unit, Faculty of Engineering, University of Mons, 7000 Mons, Belgium*
[c] *LAMSIN (LR-99-ES20), ENIT, University of Tunis El Manar, 1002 Tunis, Tunisia*
[d] *Department of Control Engineering and System Analysis, Université libre de Bruxelles, Belgium*

ARTICLE INFO

Article history:
Received 21 September 2018
Received in revised form 3 April 2019
Accepted 3 July 2019

Keywords:
Mathematical modeling
Parameter estimation
Identifiability
Maximum likelihood principal component analysis
Optimal control
Prontryagin maximum principle

ABSTRACT

The first objective of this study is to derive a macroscopic dynamic model of the production of Fructo-Oligosaccharides (FOS) by *Aureobasidium pullulans* based on sets of experimental data collected from batch and fed-batch cultures. The model should be of low dimension, so as to be identifiable based on the available data, and so as to be suitable for optimization and control purposes. A maximum likelihood principal component analysis is used to determine the appropriate number of reactions and the corresponding stoichiometry. Further, products of Monod factors are chosen to describe the reaction kinetics. The model parameters are estimated using a weighted least-squares method, and model simplification achieved by eliminating parameters associated to large uncertainties, are performed in a step-by-step, systematic way. In addition, the model structural identifiability is confirmed using generating series and the software GenSSI. Identification is successfully achieved, leading to satisfactory direct and cross-validation results. The second objective is to exploit the model and to maximize the FOS concentration at an a priori undetermined time using Pontryagin maximum principle. The optimal feed rate is in the form of a bang-bang control, which is easily implemented in practice.

1. Introduction

Fructo-oligosaccharides (FOS) are classified as prebiotics in relation with their bifidogenic nature and their health-promoting properties. FOS are gaining increasing attention in the food and pharmaceutical sectors, where they can be used to reduce levels of phospholipids, triglycerides, and cholesterol, or to help gut absorption of calcium and magnesium [23,17,1,24]. FOS can be produced from sucrose by beta-fructofuranosidase enzymes with transfructosylating and hydrolytic activity, provided by fungi, such as *Aureobasidium Pullulans* [14,31,41,12].

Only a few mathematical models of FOS production have already been published, first in [18] and [13], followed by [30] and [15]. The first model [18] considers only the synthesis reactions of FOS by fructosyltransferase, while the second [13] introduces the Nystose hydrolysis reaction. The fermentative process based on cultures of *Aureobasidium Pullulans* is described in [30,15]. The model includes biomass growth, and 1-Kestose and 1-Fructosylfuranosyl Nystose hydrolysis reactions. To the best of our knowledge, this latter model is the most detailed one and provides satisfactory prediction results. However, because of its complexity, it involves 8 state variables and 27 parameters, which require informative data sets to be estimated with reasonable accuracy and precision. As a matter of fact, with the exception of our preliminary work in [15], little attention has been paid in previous reports to the issue of parameter identifiability and the design of experiments to reduce parameter uncertainties. Starting from the detailed model, a possible investigation avenue would indeed be the use of sensitivity analysis and model reduction techniques to possibly derive a more tractable version of the biological model containing less states and parameters. Here, we favour another approach where we directly derive a (possibly low dimensional) macroscopic model of the bioprocess using data-driven techniques, and estimate the unknown parameters from experimental data. To this end, a Maximum Likelihood

* Corresponding author.
E-mail addresses: radhouane.fekihsalem@isima.rnu.tn (R. Fekih-Salem), julien.schorsch@ulb.ac.be (J. Schorsch), laurent.dewasme@umons.ac.be (L. Dewasme), cristiana.castro@umons.ac.be (C. Castro), anne-lise.hantson@umons.ac.be (A.-L. Hantson), michel.kinnaert@ulb.ac.be (M. Kinnaert), alain.vandewouwer@umons.ac.be (A. Vande Wouwer).

https://doi.org/10.1016/j.jprocont.2019.07.001
0959-1524/

Nomenclature

GF	sucrose concentration ($g\,L^{-1}$)
GF_{in}	inlet sucrose concentration ($g\,L^{-1}$)
GF_2	1-kestose concentration ($g\,L^{-1}$)
GF_3	nystose concentration ($g\,L^{-1}$)
GF_4	fructofuranosylnystose concentration ($g\,L^{-1}$)
F	fructose concentration ($g\,L^{-1}$)
G	glucose concentration ($g\,L^{-1}$)
X	biomass concentration ($g\,L^{-1}$)
r_j	reaction rates j ($g\,L^{-1}\,h^{-1}$)
k_{ij}	pseudo-stoichiometric coefficients associated to component i in reaction j
μ_j^{Max}	maximum rate of reaction j ($g\,L^{-1}\,h^{-1}$)
$K_{m_{ij}}$	Michaelis-Menten constant associated to component i in reaction j ($g\,L^{-1}$)
V	culture volume (L)
Q_{in}	inlet flow rate ($L\,h^{-1}$)
Q_{out}	outlet flow rate ($L\,h^{-1}$)
D	dilution rate (h^{-1})

Principal Component Analysis (MLPCA) approach developed in [21] is used to estimate the reaction stoichiometry independently of the kinetics. Indeed, the use of Principal Component Analysis (PCA) dates back to the seminal work of Pearson [26] and has, since then, been one of the most powerful data-driven tools to fit linear models to a set of experimental data. In [6], a methodology to determine the minimum number of reactions to describe a set of experimental data was first proposed. Based on the work of Wentzell et al. [39], Mailier et al. [21] provided a geometrical interpretation of the methodology and extended the approach to the case where the experimental datasets are corrupted by significant noise levels, in the spirit of maximum likelihood estimation.

In this study, this latter approach is applied to data sets collected from a FOS production process by *Aureobasidium pullulans* in batch and fed-batch cultures, so as to deduce a low dimension model of these cultures. The kinetics are formulated as simple products of Monod factors, and structural identifiability is checked using generating series and the software GenSSI. The model parameters are estimated using a weighted least-squares method.

Generally, practical identiability of the model parameters can be assessed using global and local sensitivity analysis (see for instance, [2,33,20,16] for a good overview of global sensitivity analysis, and [40,22] for local sensitivity analysis applied to (bio)chemical processes/systems). The Fisher Information Matrix allows assessing uncertainties on the parameters and in turn confidence intervals [28].

Direct and cross validation results demonstrate that the resulting model is able to reproduce satisfactorily the experimental data. Based on this dynamic model, an optimization strategy is developed to maximize the FOS concentration in fed-batch operation by acting on the substrate feed rate, as introduced in [32]. Since this optimal control problem is singular, the optimization is achieved by applying Pontryagin maximum principle (see, e.g., [8,35,34]). A comparison with a standard numerical procedure is carried out, validating the obtained results and demonstrating the power of the proposed approach.

The paper is organized as follows. The next section describes the experiments performed in batch and fed-batch cultures of *Aureobasidium pullulans*. In Section 3, a mathematical model is inferred from the available data sets in a two-stage procedure. First, MLPCA is used to determine the minimum number of reactions representing the data sets and the corresponding stoichiometry. Then, a simple candidate kinetic model structure is proposed in Section 4. Parameter estimation is tackled in Section 5, and the dynamic model is progressively simplified based on three successive identification steps, and the elimination of parameters associated to large uncertainties. Section 6 investigates the question of structural identifiability of the resulting dynamic model, i.e., assess the possibility of identifying the model parameters in the (theoretical) situation where perfect experimental data is available (continuous measurement of all the component concentrations), and presents cross-validation and confidence intervals. Optimal control of a fed-batch culture is achieved in Section 7 using nonlinear programming and Pontryagin maximum principle, which allows elegant results to be obtained in a simple way. Finally, conclusions are drawn in Section 8.

Table 1
Initial conditions $GF(0)$ during batch experiments ($g\,L^{-1}$).

Batch experiments	B1	B2	B3	B4
$GF(0)$	206.59	205.94	172.11	212.79

Table 2
Inlet and initial conditions of GF during fed-batch experiments ($g\,L^{-1}$).

Fed-batch experiments	FB1	FB2
$GF(0) = GF_{in}$	200.63	102.62

2. Experimental field

Experimental data originates from batch and fedbatch cultures of *Aureobasidium Pullulans* in a Sartorius BIOSTAT B+ 5L-bioreactor. The measured variables are sucrose GF, fructose F, glucose G and FOS which include 1-kestose GF_2, nystose GF_3 and fructofuranosylnystose GF_4. Since fungi grow in a heterogeneous form, it is difficult to measure the biomass X and therefore this information is not available. However, biomass evolution is slower than the above-mentioned components, and is therefore assumed in quasi steady-state (slow-fast approximation). Tables 1 and 2 describe the experimental field, i.e., the several batch and fed-batch experimental conditions with only one distinctive feature: the initial condition of GF. In batch mode, experiments B1 and B2 are used for identification and direct validation. Data was collected with a varying measurement sampling time from 2 to 10 h during the first phase of sucrose transformation (up to almost 50 h). Then, fewer samples were taken, e.g., every 6 to 16 h as the sucrose converges towards a stationary state. On the other hand, batches B3 and B4 are used for cross-validation. In this case, data sampling occurred every 5 to 15 h. In fed-batch experiments (FB1 and FB2), more frequent samples were taken (from 1 to 15 h sampling period) and a time-varying inlet flow rate $Q_{in}(\cdot)$ (1) was programmed in a stepwise manner. The inlet and initial medium concentrations were the same, i.e., $GF(0) = GF_{in}$.

These latter experiments are also used for identification and direct validation, in combination with B1 and B2 (i.e., a total of 4 experiments are used for identification, and 2 independent experiments are used for cross-validation). Fed-batch experiments usually cover a larger range of experimental conditions, carrying more information on the different (bio)chemical phenomena and should therefore be preferred to batch datasets for identification purpose. The selected data partitioning consists in 2 batch and 2 fed-batch experiments dedicated to direct validation while the 2 remaining batch cultures are used in cross-validation.

In a previous work [15], experiment design based on simulation studies suggested that the volumetric flow rate Q_{in} ($L\,h^{-1}$) in the

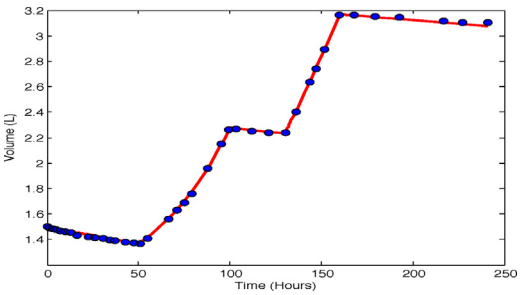

Fig. 1. Culture volume evolution in response to the applied flow rates ((1, 3)) flow rates.

fed-batch experiments should follow a combination of linear and exponential trajectories:

$$Q_{in}(t) = \begin{cases} 0 & \text{for } t \in [t_0, t_1[\cup [t_2, t_3[\cup [t_4, t_f[, \\ Q_0 e^{\beta t} & \text{for } t \in [t_1, t_2[, \\ Q_1 + \gamma t & \text{for } t \in [t_3, t_4[, \end{cases} \tag{1}$$

with, for instance, $t_0 = 0$, $t_1 = 50$, $t_2 = 100$, $t_3 = 130$, $t_4 = 160$ and $t_f = 240(h)$, so as to explore a relatively large operation range and generate informative data. Constraints on the volume can also be taken into account, the upper bound being 3.5 L. For all $t \in [t_0, t_f]$:

$$\int_{t_0}^{t} dV = \int_{t_1}^{t_2} Q_0 e^{\beta x} dx + \int_{t_3}^{t} (Q_1 + \gamma x) dx = \frac{Q_0}{\beta}(e^{\beta t_2} - e^{\beta t_1}) + Q_1(t - t_3) + \frac{\gamma}{2}(t^2 - t_3^2) \tag{2}$$

For $V(t_0) = 1.5$ L and $V(t_f) = 3.5$ L, a straightforward calculation shows that $Q_0 = 0.0043\,\mathrm{L\,h^{-1}}$ when $\beta = 0.02$ and $\gamma = 2 \times 10^{-4}$ are fixed and $Q_0 = Q_1$. Fig. 1 illustrates the volume variation according to the chosen flow rates (1) and modeling the volume withdrawal due to sampling by an equivalent output flow rate $Q_{out}(t)$ ($\mathrm{L\,h^{-1}}$) given by the following stepwise function:

$$Q_{out}(t) = \begin{cases} 2.70 \text{ mL} & \text{for } t \in [t_0, t_1[, \\ 1.74 \text{ mL} & \text{for } t \in [t_1, t_2[, \\ 1.60 \text{ mL} & \text{for } t \in [t_2, t_3[, \\ 2.10 \text{ mL} & \text{for } t \in [t_3, t_4[, \\ 1.10 \text{ mL} & \text{for } t \in [t_4, t_f[. \end{cases} \tag{3}$$

The experimental data of batch experiments (B1 and B2 of Table 1) and fed-batch experiments (FB1 and FB2 of Table 2) is shown in Fig. 3 and the following ones.

3. Model derivation

Based on the experimental data sets described in the previous section, a mathematical model structure is derived in a systematic way. The first step is the inference of the minimal number of pseudo-reactions using principal component analysis, while the second step is the deduction of a plausible kinetic structure. In this procedure, which is essentially data-driven and as systematic as possible, prior biological knowledge is of course exploited whenever available.

3.1. Determination of the minimal reaction scheme

In this section, the reaction number and stoichiometric matrix are estimated using the MLPCA-based approach described in [21]. First, we recall the concept of macroscopic reaction scheme introduced by Bastin and Dochain [4].

$$\sum_{i \in R_m} (-k_{i,m}) \xi_i \rightarrow r_m \sum_{j \in P_m} k_{j,m} \xi_j, \quad m \in [1, \ldots, N_r]. \tag{4}$$

This scheme contains N_r irreversible reactions in which appear N_ξ components denoted $\underline{\xi}$ (with, by hypothesis, $N_\xi \geq N_r$). R_m and P_m represent the set of indices i of the components $\underline{\xi}$ which are reactants and products, respectively, in reaction m. The parameters $k_{i,m}$ are pseudo-stoichiometric coefficients, while r_m is the rate of reaction m, i.e., the number of times it occurs per unit time per unit volume. Mass balance ordinary differential equations are given by:

$$\frac{d\underline{\xi}(t)}{dt} = K \underline{r}\left(\underline{\xi}\right) + \underline{\mathfrak{F}}(t) - D(t)\underline{\xi} \tag{5}$$

where $\underline{\mathfrak{F}}(t)$ is the vector of input feed rates and $D(t)$ the dilution rate. Subtracting the transportation terms and integrating the general model (5) from time 0 to time t allows to define the "transport-free" state,

$$\underline{\xi}_f(t) = \underline{\xi}(t) - \int_0^t \left[\underline{\mathfrak{F}}(\tau) - D(\tau)\underline{\xi}(\tau)\right] d\tau \tag{6}$$

whose trajectory can be computed by

$$\underline{\xi}_f(t) = \underline{\xi}(0) + K \int_0^t \underline{r}\left(\underline{\xi}(\tau)\right) d\tau \tag{7}$$

To eliminate the initial condition, a differential transport-free state vector can be considered instead

$$\underline{\xi}_f^{\Delta} := \underline{\xi}_f(t_{j+1}) - \underline{\xi}_f(t_j) = K \int_{t_j}^{t_{j+1}} \underline{r}\left(\underline{\xi}(\tau)\right) d\tau \tag{8}$$

which appears to have a trajectory included in a subspace spanned by the column vectors of the stoichiometric matrix K. This geometrical interpretation is developed in [21], where it is shown that Maximum Likelihood Principal Component Analysis allows to select the reaction number by testing the hypothesis of a dimensionality p of the candidate stoichiometric subspace, starting from $p = 1$ and increasing this dimension in the course of the successive tests. Therefore, a systematic procedure can be developed, which selects the smallest value of p that allows a thorough interpretation of the data up to a given confidence level, minimizing a log-likelihood cost:

$$J_p = \sum_{j=1}^{N_s} \left(\underline{\xi}_{f,m_i}^{\Delta} - \hat{\underline{\xi}}_f^{\Delta p}\right)^T \left(Q_j^{\Delta}\right)^{-1} \left(\underline{\xi}_{f,m_i}^{\Delta} - \hat{\underline{\xi}}_f^{\Delta p}\right) \tag{9}$$

where N_s is the number of samples, $\underline{\xi}_{f,m_i}^{\Delta}$ is the noisy measurement of $\underline{\xi}_f^{\Delta}$, Q_j^{Δ} is the covariance matrix of the measurement noise, and $\hat{\underline{\xi}}_f^{\Delta p}$ is a maximum-likelihood (ML) estimate (belonging to a p-dimensional linear model). A value of J_p larger than $\chi^{2,1-\alpha}_{N_\xi \times (N_s - 1)}$, the chi-square distribution of the normally-distributed noise realization J^* (such that $J_p \leq J^* \leq \chi^{2,1-\alpha}_{N_\xi \times (N_s-1)}$), leads to the rejection of the hypothesis $N_r = p$ at the significance level α. The reader may refer to [21] for more detailed explanations.

This methodology is now applied to the data sets collected from batch and fed-batch cultures. Fig. 2 shows that a 4-dimensional subspace (i.e., $p = 4$ reactions) is sufficient to interpret the data, which is smaller than the number of reactions considered in previous FOS production models [25,15]. Fig. 2 can indeed be analyzed as follows: (a) $N_r = p = 1, 2$ is rejected at the significance level 99.9% (almost always) and the model structure does not allow the resulting MLPCA errors to be smaller than the assumed measurement

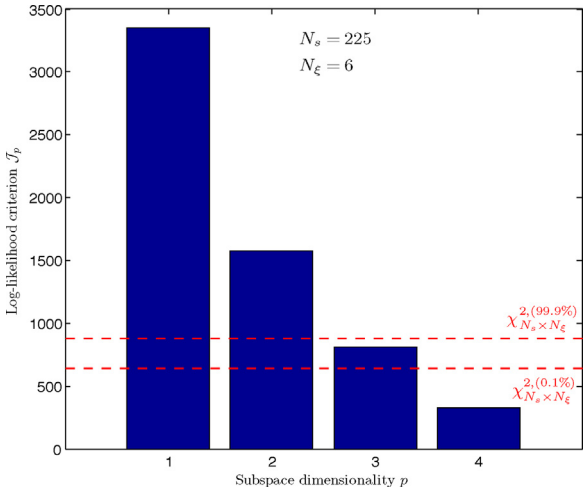

Fig. 2. *Log-likelihood* costs related to the MLPCA estimated subspaces with the data set in batch and fed-batch culture. The upper dashed line represents the chi-square quantile χ^2_{1350} at 99.9% and the lower one the chi-square quantile χ^2_{1350} at 0.1%.

noise errors. (b) $N_r = p = 3$ is rejected at the significance level 0.01% but not at 99.9% and more quantiles should be calculated to exactly determine the minimum significance level of rejection. (c) $N_r = p = 4$ is not rejected at the significance level 0.01%, i.e., the probability of $J_p \leq J^*$ to be true is smaller than 0.01% and the 4-dimensional subspace has therefore a probability of more than 99.9% to be a good model basis candidate.

A first estimate of the stoichiometric matrix $\hat{K}$ can be obtained as follows:

$$\hat{K} = \begin{bmatrix} -0.8776 & 0.2108 & -0.3415 & -0.0011 \\ 0.1141 & -0.2473 & 0.1159 & 0.5991 \\ 0.0668 & -0.2452 & -0.6593 & 0.5560 \\ 0.0402 & -0.1061 & -0.1778 & -0.1966 \\ 0.1897 & 0.8941 & 0.0199 & 0.3641 \\ 0.4180 & 0.1538 & -0.6350 & -0.4009 \end{bmatrix} \tag{10}$$

This estimate has to be examined with regards to the following points:

- Reactions should lead to the cascade synthesis of *FOS* so that *GF* and GF_2 should be the main reactant and product of the first reaction, respectively, GF_2 and GF_3 the main components of the second reaction, GF_3 and GF_4 the main components of the third one, while also allowing *FOS* hydrolysis, i.e., recovery of sucrose *GF* from *FOS* in the fourth reaction;
- Each reaction stoichiometry could be normalized with respect to the main reactant.

The first concern leads to the multiplication of the last two columns of $\hat{K}$ by -1 in order to reverse the direction of the corresponding reactions, and the reordering of the columns to match the logical reaction sequence:

$$\hat{K} = \begin{bmatrix} -0.8776 & 0.3415 & 0.0011 & 0.2108 \\ 0.1141 & -0.1159 & -0.5991 & -0.2473 \\ 0.0668 & 0.6593 & -0.5560 & -0.2452 \\ 0.0402 & 0.1778 & 0.1966 & -0.1061 \\ 0.1897 & -0.0199 & -0.3641 & 0.8941 \\ 0.4180 & 0.6350 & 0.4009 & 0.1538 \end{bmatrix}. \tag{11}$$

The second manipulation aims at eliminating artificial degrees of freedom by an adequate normalization:

$$\hat{K} = \begin{bmatrix} -1 & 2.9462 & 0.0019 & 1.9864 \\ 0.13 & -1 & -1.0775 & -2.3309 \\ 0.0762 & 5.6886 & -1 & -2.3104 \\ 0.0458 & 1.5339 & 0.3535 & -1 \\ 0.2161 & -0.1716 & -0.6548 & 8.4263 \\ 0.4763 & 5.4788 & 0.722 & 1.4492 \end{bmatrix}$$

$$= \begin{bmatrix} -1 & k_{12} & k_{13} & k_{14} \\ k_{21} & -1 & -k_{23} & -k_{24} \\ k_{31} & k_{32} & -1 & -k_{34} \\ k_{41} & k_{42} & k_{43} & -1 \\ k_{51} & -k_{52} & -k_{53} & k_{54} \\ k_{61} & k_{62} & k_{63} & k_{64} \end{bmatrix}. \tag{12}$$

This formatted estimate will serve as a starting point for the subsequent model parameter identification. The reaction scheme with generic parameters can be written as:

$$\begin{aligned} GF &\xrightarrow{r_1} k_{21}GF_2 + k_{31}GF_3 + k_{41}GF_4 + k_{51}F + k_{61}G \\ GF_2 + k_{52}F &\xrightarrow{r_2} k_{12}GF + k_{32}GF_3 + k_{42}GF_4 + k_{62}G \\ k_{23}GF_2 + GF_3 + k_{53}F &\xrightarrow{r_3} k_{13}GF + k_{43}GF_4 + k_{63}G \\ k_{24}GF_2 + k_{34}GF_3 + GF_4 &\xrightarrow{r_4} k_{14}GF + k_{54}F + k_{64}G. \end{aligned} \tag{13}$$

4. Kinetic model formulation

Considering

$$\underline{\xi}^T(t) = \left[\xi_1, \xi_2, \ldots, \xi_7\right] = [GF, GF_2, GF_3, GF_4, F, G, V] \tag{14}$$

as the state vector, a simple candidate kinetic structure is suggested as:

$$r_j(\xi_1, \xi_2, \ldots, \xi_6) = \mu_j^{Max} \prod_{i \in R_j^*} \frac{\xi_i(t)}{K_{m_{ij}} + \xi_i(t)}, \quad j = 1, \ldots, 4 \tag{15}$$

with μ_j^{Max} the maximum rate of reaction j, $K_{m_{ij}}$ the Michaelis-Menten constant associated to component i in reaction j, and R_j^* the set of reactants in reaction j. More precisely, one has

$$r_1 = \mu_1^{Max} \frac{GF}{K_{m_{11}} + GF}, \quad r_2 = \mu_2^{Max} \frac{GF_2}{K_{m_{22}} + GF_2} \frac{F}{K_{m_{52}} + F}, \tag{16}$$

$$\begin{aligned} r_3 &= \mu_3^{Max} \frac{GF_2}{K_{m_{23}} + GF_2} \frac{GF_3}{K_{m_{33}} + GF_3} \frac{F}{K_{m_{53}} + F}, \\ r_4 &= \mu_4^{Max} \frac{GF_2}{K_{m_{24}} + GF_2} \frac{GF_3}{K_{m_{34}} + GF_3} \frac{GF_4}{K_{m_{44}} + GF_4}. \end{aligned} \tag{17}$$

Hence, the model includes 13 kinetic parameters and 20 pseudo-stoichiometric coefficients:

$$\begin{cases} \dot{GF} = D(GF_{in} - GF) - r_1 + k_{12}r_2 + k_{13}r_3 + k_{14}r_4 \\ \dot{GF}_2 = -D.GF_2 - r_2 + k_{21}r_1 - k_{23}r_3 - k_{24}r_4 \\ \dot{GF}_3 = -D.GF_3 - r_3 + k_{31}r_1 + k_{32}r_2 - k_{34}r_4 \\ \dot{GF}_4 = -D.GF_4 - r_4 + k_{41}r_1 + k_{42}r_2 + k_{43}r_3 \\ \dot{F} = -D.F + k_{51}r_1 - k_{52}r_2 - k_{53}r_3 + k_{54}r_4 \\ \dot{G} = -D.G + k_{61}r_1 + k_{62}r_2 + k_{63}r_3 + k_{64}r_4 \\ \dot{V} = Q_{in} - Q_{out}, \end{cases} \tag{18}$$

where GF_{in} denotes the inlet GF concentration, Q_{in} and Q_{out} represent the inlet and outlet flow rates, respectively, and $D = \frac{Q_{in}}{V}$ the dilution rate. The following proposition shows that system (18) is behaving as well as one would expect for any reasonable biological model.

Proposition 1. *For any nonnegative initial condition, the solutions of (18) remain nonnegative.*

Proof. From (16) and (17), the growth rate $\underline{r}(\underline{\xi})$ can be rewritten as:

$$\underline{r}(\underline{\xi}) = G(\underline{\xi})\underline{\alpha}, \tag{19}$$

with the vector of nonlinear functions $\underline{\alpha}^T = [\alpha_1(GF), \alpha_2(GF_2, F), \alpha_3(GF_2, GF_3, F), \alpha_4(GF_2, GF_3, GF_4)]$ and

$$G(\underline{\xi}) = \begin{bmatrix} GF & 0 & 0 & 0 \\ 0 & GF_2 \;\; F & 0 & 0 \\ 0 & 0 & GF_2 \;\; GF_3 \;\; F & 0 \\ 0 & 0 & 0 & GF_2 \;\; GF_3 \;\; GF_4 \end{bmatrix} \tag{20}$$

Let $\xi_i(0) \geq 0$, $i = 1, \ldots, N_y$. At the first time instant $t^* \geq 0$ where $\xi_i(t^*) = 0$, it follows from (5) and (19)

$$\dot{\xi}_i(t*) = \sum_{j=1}^{4} k_{ij}G_{jj}(\underline{\xi})\alpha_j - D(t)\underline{\xi}(t*) + \mathfrak{F}_i(t*). \tag{21}$$

Since all terms in the right-hand side of (21) are nonnegative, $\xi_i(t) \geq 0$ for all $t \geq t^*$. Indeed, if $k_{ij} < 0$ for some j (i.e., $\xi_i(t^*)$ is a reactant in the jth reaction), $G_{jj}(\underline{\xi}) = 0$ from (20). Obviously, $\xi_i(t) \geq 0$ for all $t \in [0, t^*]$, thus $\xi_i(t) \geq 0$ for all $t \geq 0$.

5. Nonlinear parameter estimation

Model (18) is a nonlinear differential equation system of the form

$$\frac{d\underline{\xi}(t)}{dt} = \underline{f}\left(\underline{\xi}(t), \underline{u}(t); \underline{\theta}\right), \tag{22}$$

where $\underline{\xi}^T(t)$ is the state vector defined in (14), $\underline{u}(t) = \left[D(t) \;\; \underline{\mathfrak{F}}^T(t)\right]$ is a vector containing the inputs to the bioreactor, and

$$\underline{\theta} = \left[\underline{\theta}_r^T \;\; \underline{\theta}_K^T \;\; \underline{\xi}_1^T(0) \cdots \underline{\xi}_{N_{\exp}}^T(0)\right] \tag{23}$$

is a vector of unknown parameters ($\underline{\theta} \in \mathbb{R}^{N_p}$), where $\underline{\theta}_r$ is the vector of kinetic parameters (in this study $dim\left(\underline{\theta}_r\right) = 13$), $\underline{\theta}_K$ the vector of stoichiometric parameters ($dim\left(\underline{\theta}_K\right) = 20$), $\underline{\xi}_j(0)$, $j = 1, \ldots, N_{exp}$, are the initial conditions (concentrations and volume in fed-batch) of the jth experiment, which can be considered as parameters to be identified. Finally, N_{exp} denotes the number of experiments.

The following solution $\underline{y}_j^{sim}$ (where j stands for the experiment number) of model (22) can be obtained through numerical integration, for instance using an ODE solver from Matlab, and depends on the parameter set $\underline{\theta}$

$$\underline{y}_j^{sim}\left(t; \underline{\theta}\right) = \underline{g}_j\left(\underline{\xi}(t), \underline{u}(t); \underline{\theta}\right), \quad j = 1, \ldots, N_{\exp} \tag{24}$$

On the other hand, the vector of data collected at times t_{ij} is given by:

$$\underset{-j}{y}^{\exp}\left(t_{ij}\right) = \underset{-j}{y}^{sim}\left(t_{ij}; \underset{-}{\theta}^*\right) + \underset{-ij}{\eta}, \quad j = 1, \ldots, N_{\exp}, \quad i = 1, \ldots, N_{t_j} \tag{25}$$

where t_{ij} denotes the ith sample time of the jth experiment, $\underline{y}_j^{\exp}$ the corresponding measurement vector and N_{t_j} represents the total number of sampling times of the jth experiment. If the model structure is appropriate (no characterization error), $\underline{\theta}^*$ represents the (hypothetically) true value of the parameter vector. The measurement errors are assumed to be independent, zero mean and Gaussian,

$$\underset{-ij}{\eta} \hookrightarrow N\left(0, \Sigma_j\right), \quad j = 1, \ldots, N_{\exp}, \quad i = 1, \ldots, N_{t_j} \tag{26}$$

In practice, in the absence of a priori knowledge on the measurement error statistics, a pragmatic approach consists in using the *Weighted Least Squares* (WLS) criterion, where the cost function $J\left(\underline{\theta}\right)$ is given by

$$J\left(\underline{\theta}\right) = \sum_{j=1}^{N_{\exp}} J_j\left(\underline{\theta}\right), \tag{27}$$

with

$$J_j\left(\underline{\theta}\right) = \sum_{i=1}^{Nt_j} \left[\underline{y}_j^{\exp}\left(t_{ij}\right) - \underline{y}_j^{sim}\left(t_{ij}; \underline{\theta}\right)\right]^T W_j^{-1} \left[\underline{y}_j^{\exp}\left(t_{ij}\right) - \underline{y}_j^{sim}\left(t_{ij}; \underline{\theta}\right)\right], \tag{28}$$

and W_j, a semi-positive-definite symmetric weighting matrix defined by

$$W_j = \text{diag}\left(\max_{1 \leq i \leq Nt_j}\left(y_{j1}^{\exp}\left(t_{ij}\right)\right)^2, \ldots, \max_{1 \leq i \leq Nt_j}\left(y_{jN_{y_j}}^{\exp}\left(t_{ij}\right)\right)^2\right), \quad j = 1, \ldots, N_{\exp} \tag{29}$$

In the absence of precise knowledge of the measurement noise distribution, the selection of a diagonal weighting matrix, with the squared maximum of the measured variables (e.g., concentrations) on the diagonal, allows a scaling of the data (units and ranges). Keeping the statistical interpretation in mind, this matrix also considers the possibility of relative errors in the data.

The WLS estimator

$$\hat{\underline{\theta}} = arg\min_{\underline{\theta}} J\left(\underline{\theta}\right) \tag{30}$$

is obtained using numerical optimization. In this study, a procedure combining Nelder-Mead with Quasi-Newton optimization is used (e.g., fminsearchbnd as implemented in Matlab when starting from the initial parameter guess, followed by fminunc in the neighbourhood of the solution).

The a posteriori covariance matrix of the measurement noise of the jth experiment can be estimated by $\hat{\Sigma}_j = \hat{\epsilon}_j^2 W_j$ where the measurement error variance of the jth experiment $\hat{\epsilon}_j^2$ is given by

$$\hat{\epsilon}_j^2 = \frac{J_j(\hat{\underline{\theta}})}{N_{y_j}N_{t_j} - N_p}, \quad j = 1, \ldots, N_{\exp} \tag{31}$$

The parametric sensitivities

$$S_\theta\left(t, \underline{u}(t); \underline{\theta}\right) = \frac{\partial \underline{\xi}\left(t; \underline{\theta}\right)}{\partial \underline{\theta}} \tag{32}$$

are useful to assess parameter identifiability and to evaluate confidence intervals. It can be computed through the solution of the following sensitivity equations obtained by differentiating the model equations with respect to the parameters

$$\frac{\partial S_\theta\left(t,\underline{u}(t);\underline{\theta}\right)}{\partial t}=\frac{\partial \underline{f}\left(\underline{\xi}(t),\underline{u}(t);\underline{\theta}\right)}{\partial \underline{\xi}}S_\theta\left(t,\underline{u}(t);\underline{\theta}\right)+\frac{\partial \underline{f}\left(\underline{\xi}(t),\underline{u}(t);\underline{\theta}\right)}{\partial \underline{\theta}} \tag{33}$$

When considering Gaussian measurement noise, the Fisher Information Matrix (FIM) can be determined using the following equation [38]

$$\text{FIM}\left(\underline{\theta},\hat{\Sigma}\right)=\sum_{j=1}^{N_{\text{exp}}}\sum_{i=1}^{Nt_j}S_\theta^T\left(t_{ij},\underline{u}\left(t_{ij}\right);\underline{\theta}\right)\hat{\Sigma}_j^{-1}S_\theta\left(t_{ij},\underline{u}\left(t_{ij}\right);\underline{\theta}\right) \tag{34}$$

Under suitable regularity conditions, the inverse of the FIM provides an optimistic estimate (Cramér-Rao bound) of the parameter error covariance matrix [38]

$$C_{\underline{\theta}}\geq \text{FIM}^{-1}\left(\hat{\underline{\theta}},\hat{\Sigma}\right). \tag{35}$$

The standard deviation σ_k of the parameter estimates $\hat{\underline{\theta}}_k$ can be obtained from the square root of the *kth* diagonal element of $C_{\underline{\theta}}$

$$\sigma_k=\sqrt{C_{\underline{\theta}_{kk}}},\quad k=1,\ldots,N_p \tag{36}$$

and a 95% confidence confidence interval can be estimated by

$$\left[\hat{\theta}_k-2\sigma_k,\hat{\theta}_k+2\sigma_k\right],\quad k=1,\ldots,N_p \tag{37}$$

Strong correlation between parameters can however lead to the singularity of the FIM matrix and consequently, which is a visible sign of non-identifiability of the parameters. The reciprocal condition number (RCN computed using rcond in Matlab) can be used to assess matrix singularity (a well-conditioned matrix has RCN close to 1, whereas a badly-conditioned matrix has RCN close to zero). If

$$\text{rcond(FIM)}<10\times\varepsilon, \tag{38}$$

where ε is the floating point relative accuracy (2.2×10^{-16}), the FIM is considered singular.

5.1. First identification step

The parameters of model (18) are estimated using the above mentioned procedure and the results are shown in Table 3. In this table, the variation coefficients are given by the ratio of the standard deviation σ_k to the respective parameter estimate $\hat{\underline{\theta}}_k$.

The stoichiometry may appear different from (12), which was determined by MLPCA independently of the formulation of the kinetics. Matrix (12) is considered here as a first guess in the identification procedure. The low values, and relatively large uncertainty intervals, of the pseudo-stoichiometric coefficients $k_{12}, k_{13}, k_{24}, k_{41}$, k_{52}, k_{62}, and k_{64} lead to their elimination from the model.

Hence, the pseudo-stoichiometric matrix (12) becomes:

$$\hat{K}=\begin{bmatrix}-1 & 0 & 0 & k_{14}\\ k_{21} & -1 & -k_{23} & 0\\ k_{31} & k_{32} & -1 & -k_{34}\\ 0 & k_{42} & k_{43} & -1\\ k_{51} & 0 & -k_{53} & k_{54}\\ k_{61} & 0 & k_{63} & 0\end{bmatrix}. \tag{39}$$

The corresponding reaction scheme

$$\begin{aligned} GF &\xrightarrow{r_1} k_{21}GF_2+k_{31}GF_3+k_{51}F+k_{61}G\\ GF_2 &\xrightarrow{r_2} k_{32}GF_3+k_{42}GF_4\\ k_{23}GF_2+GF_3+k_{53}F &\xrightarrow{r_3} k_{43}GF_4+k_{63}G\\ k_{34}GF_3+GF_4 &\xrightarrow{r_4} k_{14}GF+k_{54}F \end{aligned} \tag{40}$$

involves the simplified reaction rates

$$r_2=\mu_2^{Max}\frac{GF_2}{K_{m_{22}}+GF_2},\quad r_4=\mu_4^{Max}\frac{GF_3}{K_{m_{34}}+GF_3}\frac{GF_4}{K_{m_{44}}+GF_4}, \tag{41}$$

where the half-saturation coefficients $K_{m_{52}}$ and $K_{m_{24}}$ no longer appear (since F and GF_2 are no longer part of the second and fourth reactions, respectively). The model now includes 11 Kinetic parameters and 13 pseudo-stoichiometric coefficients.

Fig. 3 shows the predictive capability of model (39)–(41) in direct validation. The experimental data consist of 2 batch (B1 and B2) and 2 fed-batch (FB1 and FB2) experiments. However, the confidence intervals of some of the estimated parameters are too large (see Table 3) and rcond(FIM) = 4.95×10^{-11} (nonsingular FIM, but with a small RCN).

5.2. Second identification step

Following the model simplification, the parameters of model (39)–(41) are now re-estimated, leading to the results listed in Table 3. The pseudo-stoichiometric coefficients k_{31} and k_{42} are relatively small with respect to other coefficients in the same reactions or with respect to coefficients associated to the same component in other reactions. Coefficients k_{23} and k_{53} are significantly larger but their confidence intervals are also quite large and include zero. It is therefore decided to eliminate these 4 coefficients, and to test the following simplified model:

$$\hat{K}=\begin{bmatrix}-1 & 0 & 0 & k_{14}\\ k_{21} & -1 & 0 & 0\\ 0 & k_{32} & -1 & -k_{34}\\ 0 & 0 & k_{43} & -1\\ k_{51} & 0 & 0 & k_{54}\\ k_{61} & 0 & k_{63} & 0\end{bmatrix} \tag{42}$$

with the reaction rates

$$r_1=\mu_1^{Max}\frac{GF}{K_{m_{11}}+GF},\quad r_i=\mu_i^{Max}\frac{GF_i}{K_{m_{ii}}+GF_i},\quad i=2,3,$$
$$r_4=\mu_4^{Max}\frac{GF_3}{K_{m_{34}}+GF_3}\frac{GF_4}{K_{m_{44}}+GF_4}. \tag{43}$$

This model has 9 pseudo-stoichiometric coefficients and 9 kinetic parameters.

Table 3
Parameter estimation results for the 4 candidate models using the experimental data collected in 2 batch (B1 and B2) and 2 fed-batch (FB1 and FB2) experiments – the parameter values are given with a 95% confidence interval.

Parameter	Model (18)	Model (39)–(41)	Model (42) and (43)	Model (44) and (45)	Variation coefficient[a] (%)
μ_1^{Max}	9.34 ± 0.21	10.16 ± 0.19	8.58 ± 0.27	9.11 ± 0.31	1.7
μ_2^{Max}	1.39 ± 1.83	7.79 ± 1.33	32.96 ± 0.9	7.13 ± 0.17	1.2
μ_3^{Max}	21.1 ± 27.9	2.17 ± 2.44	7.99 ± 0.16	7.91 ± 0.12	0.8
μ_4^{Max}	0.28 ± 0.06	0.5 ± 0.03	0.22 ± 0.01	0.25 ± 0.01	2.0
Km_{11}	$10^{-4} \pm 5.72$	10.3 ± 7.49	4.06 ± 5.43	12.03 ± 7.89	32.8
Km_{22}	364.6 ± 104.5	422.18 ± 65.1	860.6 ± 80.9	140.2 ± 12.5	4.5
Km_{52}	6.3 ± 1.46				
Km_{23}	532 ± 1406	137.5 ± 240			
Km_{33}	69.1 ± 148.7	62.93 ± 84.96	41.7 ± 12.9	24.8 ± 8.9	17.9
Km_{53}	28.89 ± 45.7	37.84 ± 37.98			
Km_{24}	$10^{-3} \pm 10.7$				
Km_{34}	10.9 ± 15.3	12.36 ± 2.34	0.12 ± 1.39		
Km_{44}	0.003 ± 0.15	0.019 ± 0.16	0.86 ± 0.48	1.37 ± 0.59	21.5
k_{12}	0.04 ± 20.5				
k_{13}	$5 \times 10^{-3} \pm 14$				
k_{14}	3.59 ± 6.85	5.21 ± 0.67	5.65 ± 0.93	5.52 ± 0.76	6.9
k_{21}	0.31 ± 0.03	0.33 ± 0.02	0.43 ± 0.03	0.44 ± 0.03	3.4
k_{23}	4.89 ± 7.24	12.4 ± 14.3			
k_{24}	$10^{-3} \pm 0.95$				
k_{31}	0.11 ± 0.07	0.06 ± 0.05			
k_{32}	33.6 ± 39.9	4.45 ± 0.65	2.62 ± 0.39	3.04 ± 0.36	5.9
k_{34}	14.38 ± 2.93	7.59 ± 0.52	$4 \times 10^{-3} \pm 0.17$		
k_{41}	$10^{-4} \pm 0.009$				
k_{42}	1.22 ± 1.18	0.42 ± 0.05			
k_{43}	1.52 ± 1.7	4.96 ± 5.77	0.1 ± 0.01	0.09 ± 0.01	
k_{51}	0.03 ± 0.01	0.04 ± 0.01	0.03 ± 0.01		
k_{52}	0.011 ± 1.97				
k_{53}	1.36 ± 1.83	6.9 ± 7.99			
k_{54}	2.03 ± 0.54	1.37 ± 0.29	1.07 ± 0.22	1.27 ± 0.11	4.3
k_{61}	0.21 ± 0.05	0.21 ± 0.03	0.26 ± 0.04	0.25 ± 0.02	4.0
k_{62}	$2 \times 10^{-6} \pm 10.9$				
k_{63}	2.06 ± 4.38	0.99 ± 3.42	$2 \times 10^{-3} \pm 0.05$		
k_{64}	$5 \times 10^{-7} \pm 3.5$				

Variation coefficients of the estimated parameters of model (44) and (45).

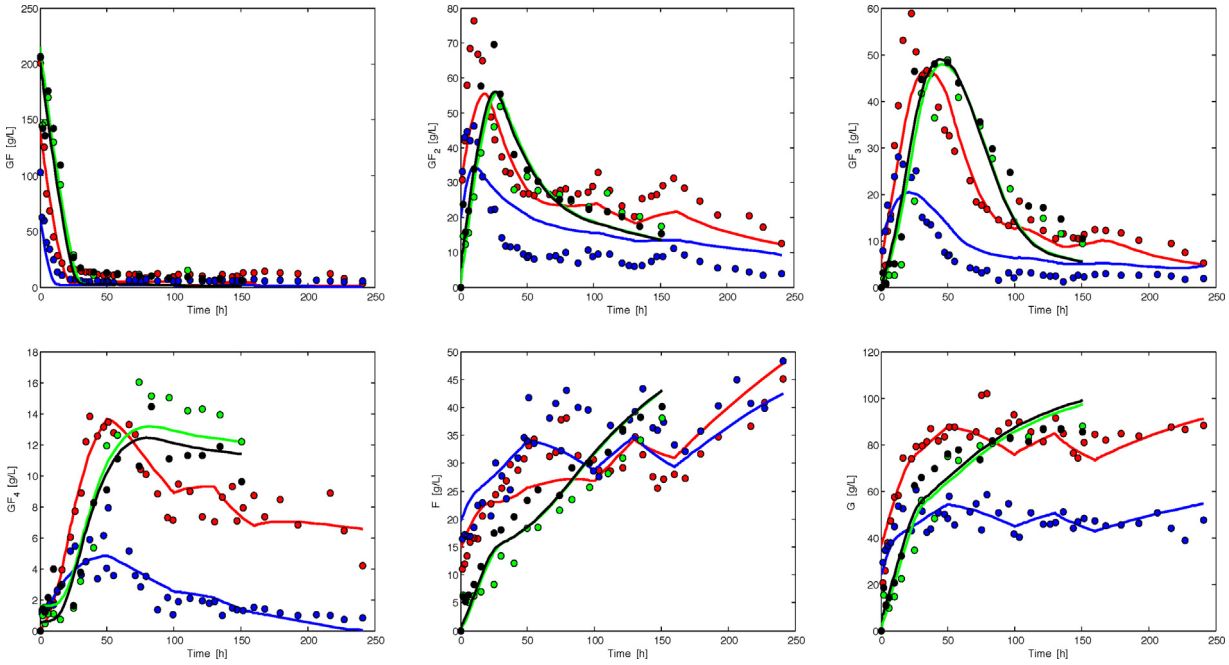

Fig. 3. Batch experiments (B1:green – B2: black) and fed-batch experiments (FB1:red – FB2:blue). Measurements and model prediction (39)–(41) where $J(\theta) = 6.59$ (RMSE=8.03). (For interpretation of the references to color in this figure legend, the reader is referred to the web version of this article.)

Fig. 4 shows the good fit of model (42) and (43) with the experimental data at hand, despite the drastic reduction of the number of parameters. Moreover, the confidence intervals of the remaining parameters are now relatively small (see Table 3). FIM is regular with rcond(FIM) = 2.34×10^{-10} (a slight improvement over the previous results).

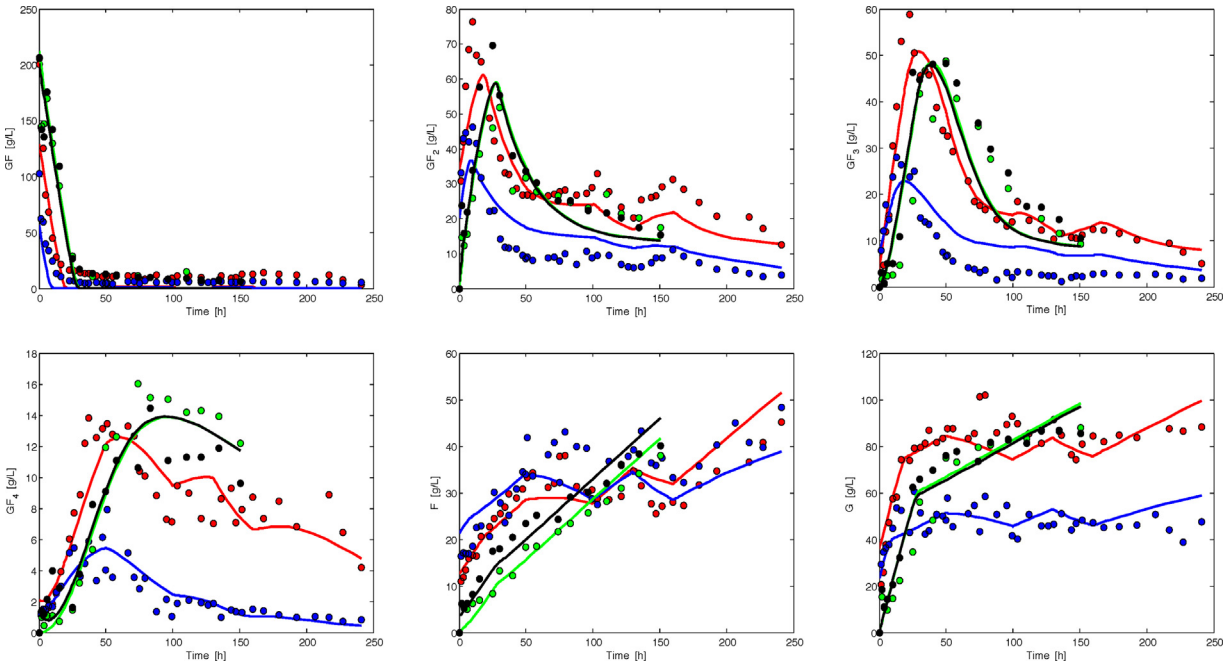

Fig. 4. Batch experiments (B1:green – B2: black) and fed-batch experiments (FB1:red – FB2:blue). Measurements and model prediction (42) and (43) where $J(\theta)=7.06$ (RMSE=8.39). (For interpretation of the references to color in this figure legend, the reader is referred to the web version of this article.)

5.3. Third identification step

Following the model simplification, the parameters of model (42) and (43) are re-estimated and listed in Table 3. Again, some pseudo-stoichiometric coefficients display small values that could open the door to further simplifications. This is the case for the pseudo-stoichiometric coefficients k_{34} and k_{63}, and to a less extent k_{51}, which are eliminated leading to:

$$\hat{K} = \begin{bmatrix} -1 & 0 & 0 & k_{14} \\ k_{21} & -1 & 0 & 0 \\ 0 & k_{32} & -1 & 0 \\ 0 & 0 & k_{43} & -1 \\ 0 & 0 & 0 & k_{54} \\ k_{61} & 0 & 0 & 0 \end{bmatrix} \tag{44}$$

$$r_1 = \mu_1^{Max}\frac{GF}{K_{m_{11}}+GF}, \quad r_i = \mu_i^{Max}\frac{GF_i}{K_{m_{ii}}+GF_i}, \quad i=2,3,4. \tag{45}$$

Hence the model has now 8 Kinetic parameters and 6 pseudo-stoichiometric coefficients.

Fig. 5 confirms the predictive capability of this last candidate model. Also, the confidence intervals and the variation coefficients of the remaining parameters are now relatively small (see Table 3), and the RCN of the FIM continues improving with $\text{rcond(FIM)} = 7.15 \times 10^{-9}$. Interestingly, the remaining stoichiometric coefficients are now much closer to the values derived by MLPCA and accepted as a first guess. This reinforces the consistency of the results.

6. Model identifiability and validation

The previous sections suggest a step-by-step model identification and reduction, based on the analysis of the parameter estimates and confidence intervals, i.e., based on practical identifiability in view of the available experimental data. This practical approach can be supplemented by a deeper theoretical analysis of the model structure, i.e., structural identifiability [38]. Assuming ideal conditions, i.e., no-error in the model structure and noise-free, time-continuous measurements, there exists an estimated parameter vector $\underline{\hat{\theta}}$ such that the model input-output behaviour is identical to that of the process, that is,

$$M(\underline{\hat{\theta}}) = M(\underline{\theta}^*) \tag{46}$$

where $\underline{\theta}^*$ denotes the (hypothetical) true value of the parameters.

- A parameter θ_i is structurally globally (or uniquely) identifiable (s.g.i) if for almost any $\underline{\theta}^*$ in the parameter space Θ,

$$M(\underline{\hat{\theta}}) = M(\underline{\theta}^*) \Rightarrow \underline{\hat{\theta}} = \underline{\theta}^* \tag{47}$$

- A parameter θ_i is structurally locally identifiable (s.l.i.) if for almost any $\underline{\theta}^* \in \Theta$, there exists a neighbourhood $\mathbb{V}(\underline{\theta}^*)$ such that

$$\underline{\hat{\theta}} \in \mathbb{V}(\underline{\theta}^*) \quad \text{and} \quad M(\underline{\hat{\theta}}) = M(\underline{\theta}^*) \Rightarrow \underline{\hat{\theta}} = \underline{\theta}^*. \tag{48}$$

- A parameter θ_i is structurally unidentifiable (s.u.i.) when Eq. (48) does not hold in any neighborhood of $\mathbb{V}(\underline{\theta}^*)$.

Several methods are available to analyze this property (see the overview in for instance [9,36]), such as: differential algebra [29], Taylor series [27] or generating series [37]. Moreover, several software tools have been developed, e.g., DAISY (differential algebra) [5], GenSSI (generating series) [10] and Observability Tool (local observability test) [19].

The nonlinear differential equations describing the biological system can usually be written in the following affine-in-the-input form:

$$M(\underline{\theta}): \begin{cases} \dot{\underline{\xi}}(t) & = \underline{f}\left(\underline{\xi}, \underline{\theta}, t\right) + \sum_{j=1}^{N_u} u_j(t)\underline{g}_j\left(\underline{\xi}, \underline{\theta}, t\right), \quad \underline{\xi}(t_0) = \underline{\xi}_0\left(\underline{\theta}\right), \\ \underline{y}\left(t, \underline{\theta}\right) & = \underline{h}\left(\underline{\xi}, \underline{\theta}, t\right) \end{cases} \tag{49}$$

where $M(\underline{\theta})$ is the model corresponding to specific parameter values $\underline{\theta}$ in the model class M, $\underline{\xi} \in \mathbb{R}^{N_\xi}$ is the vector of state variables

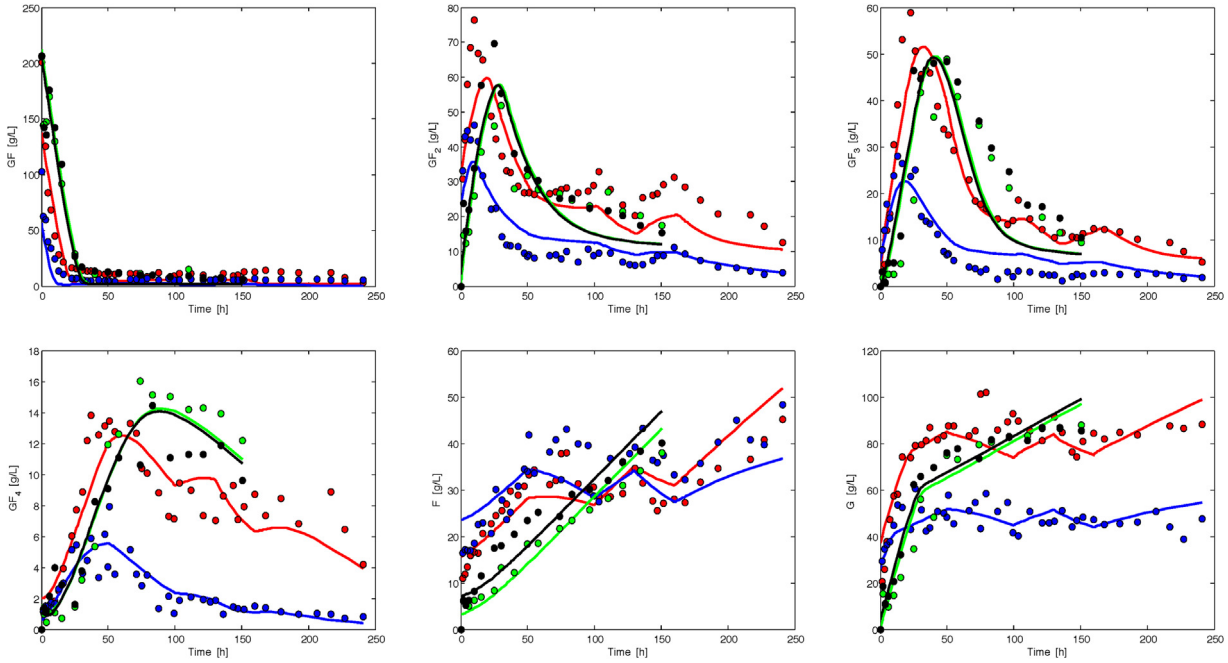

Fig. 5. Batch experiments (B1:green – B2:black) and fed-batch experiments (FB1:red – FB2:blue). Measurements and model prediction (44) and (45) where $J(\theta) = 9.41$ (RMSE=8.18). (For interpretation of the references to color in this figure legend, the reader is referred to the web version of this article.)

Table 4
Comparison of the 4 candidate models: Root-Mean-Square Error (RMSE), Number of Lie derivatives (Nder), structurally locally identifiable (s.l.i.) and structurally globally identifiable (s.g.i).

Model	RMSE	$dim\left(\underline{\theta}_r\right)$	$dim\left(\underline{\theta}_K\right)$	rcond(FIM)	Nder	s.l.i.	s.g.i
(18)	8.29	13	20	4.11×10^{-13}	memory limitation	memory limitation	memory limitation
(39)–(41)	8.03	11	13	4.95×10^{-11}	4	OK	OK
(42) and (43)	8.39	9	9	2.34×10^{-10}	3	OK	OK
(44) and (45)	8.18	8	6	7.15×10^{-9}	3	OK	OK

(concentrations), $\underline{u} \in \mathbb{R}^{N_u}$ is the vector of manipulated variables (flow rates), $\underline{y} \in \mathbb{R}^{N_y}$ is the output (measurement) vector. $\underline{\xi}_0\left(\underline{\theta}\right)$ are the initial conditions (concentrations) that may be included in the unknown parameters.

The selected method is the generating series approach, which is based on the decomposition of the output function $\underline{h}$ in series with respect to time and the inputs, whose coefficients are $\underline{h}$ and the Lie derivatives of $\underline{h}$ along the vector fields $\underline{f}$ and $\underline{g}_j$ [3,9]. For instance,

$$L_{\underline{f}}\underline{h}(\underline{\xi}(t), \underline{\theta}, t) = \sum_{j=1}^{N_\xi} f_j\left(\underline{\xi}(t), \underline{\theta}, t\right) \frac{\partial \underline{h}}{\partial \underline{\xi}_j}\left(\underline{\xi}(t), \underline{\theta}, t\right) \tag{50}$$

where f_j denotes the jth component of $\underline{f}$.

Let $s(\underline{\theta})$ be an *exhaustive summary* containing the series coefficients obtained by successive computation of Lie derivatives along $\underline{f}$ and $\underline{g}_j$ at the initial state $\underline{\xi}(t_0) = \underline{\xi}_0(\underline{\theta})$. The model is identifiable if there exists a unique solution for $\underline{\theta}$ from $s(\underline{\theta})$.

The several previous model candidates can be analyzed with the software toolbox GenSSI [10]. The results are summarized in Table 4, together with the previous results of the nonlinear parameter estimation procedure.

The structural identifiability analysis of the initial model (18) is unfortunately not possible due to memory limitation (with our computing facilities at least). Due to the model simplification, the analysis of the subsequent models, which contain less parameters, is however possible.

All the latter models are structurally globally identifiable and attention is focused on the analysis of the last, most promising one, i.e., model (44) and (45). The *identifiability tableaus* represented in Fig. 6 shows the non-zero elements of the Jacobian of the series coefficients with respect to the parameters. Each column of these tableaus corresponds to a model parameter (they have 14 columns for the model under consideration), while the rows correspond to non-zero series coefficients. If the tableau presents empty columns, the corresponding parameters may be non-identifiable (but not necessarily as the number of series coefficients can in principle be infinite, and a strict proof of non-identifiability would require a proof that higher-order coefficients are zero). Fig. 6(a) illustrates the complete identifiability tableau where at least structural local identifiability is guaranteed with 3 derivatives since there is no empty column, viz. the rank of the Jacobian corresponds to the number of parameters. Fig. 6(b) illustrates the *reduced identifiability tableau* which corresponds to the minimum number of linearly independent relations that would allow to compute the parameters [3].

6.1. Cross validation

The candidate model (44) and (45) can be cross-validated using the batch experiments B3 and B4 which have not been used in the identification process. Before proceeding to the assessment of the model predictive capability through the cross-validation, good practice suggests to identify the initial conditions of the new experiments (B3 and B4) while keeping the parameters of the model (44) and (45) fixed at their previously estimated values. Indeed, the initial measured values are perturbed by noise, which could affect the initialization of the model trajectories. The estimated initial condi-

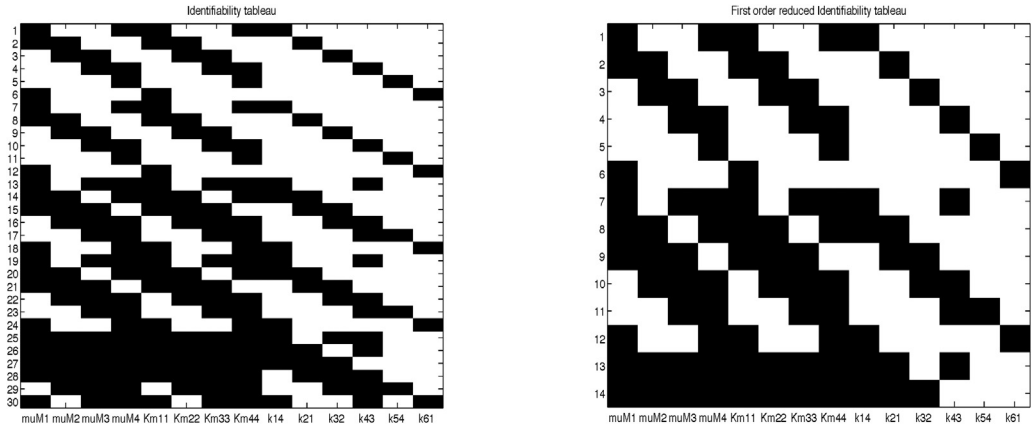

Fig. 6. Identifiability tableaus generated by the software GenSSI for model (44) and (45) with 14 parameters. A black square at the coordinates (i, j) indicates that the corresponding non-zero generating series coefficient i depends on the parameter j. The left tableau corresponds to three Lie derivatives, while the right tableau is the reduced one.

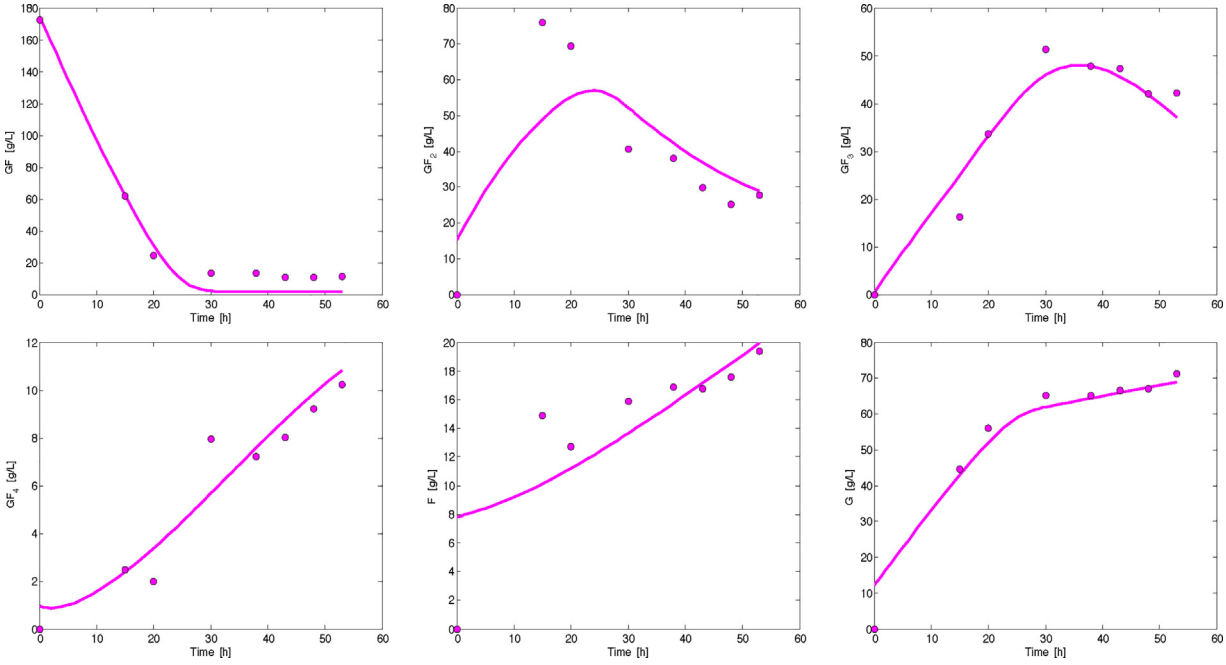

Fig. 7. Cross-validation of reduced model (44) and (45) with experiment B3 (RMSE=7.05).

Table 5
Identification of initial conditions of batch experiments B3 and B4.

Experiment	$GF(0)$	$GF_2(0)$	$GF_3(0)$	$GF_4(0)$	$F(0)$	$G(0)$
B3	174.80	15	0.22	0.96	7.78	12.05
B4	193.86	3.74	10^{-6}	0.13	9.70	34.62

tions are listed in Table 5. Figs. 7 and 8 show that the model, using the identified initial conditions, is able to reproduce relatively well new experiments.

6.2. Confidence corridors

Considering the general model (22), the parametric sensitivity equations (33) and the Fisher Information Matrix (34) in the case of Gaussian noise, it is possible to derive a first-order estimate of the covariance of the model prediction error ε_x

$$E\left[\underline{\varepsilon}_x \underline{\varepsilon}_x^T\right] = S_\theta \mathrm{FIM}^{-1} S_\theta^T + S_{\underline{x}_0} Q_0 S_{\underline{x}_0}^T. \quad (51)$$

This covariance matrix depends on the covariance of the parameters (estimated via the FIM) and the sensitivity of the model outputs to the parameters, as well as to the covariance of the (measurement) errors on the initial conditions Q_0 and the sensitivity to the initial conditions. Fig. 9 illustrates the 95%-confidence corridors related to the prediction of experiment B1 by model (44) and (45). These corridors always include the measured data, thus confirming the validity of the proposed model.

7. Optimal control of fed-batch operation

The objective of this section is to determine an optimal substrate feed rate for optimizing the FOS concentration at an undetermined final time. Several parameters have to be selected such as the feeding start time, rate, and stop time, under constraints such as the maximum volume of the bioreactor. Two approaches will be followed and compared. The first is Pontryagin maximum principle, which allows an elegant problem solution, whereas the second is straightforward and consists in a numerical optimization.

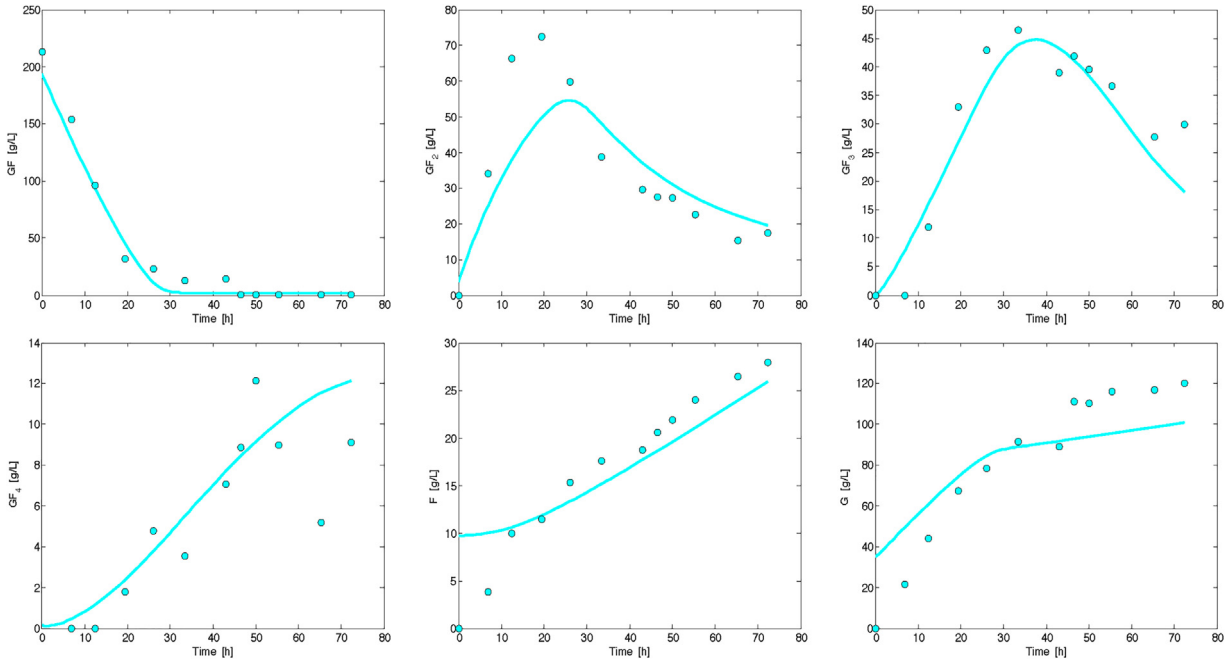

Fig. 8. Cross-validation of reduced model (44) and (45) with experiment B4 (RMSE=10.33).

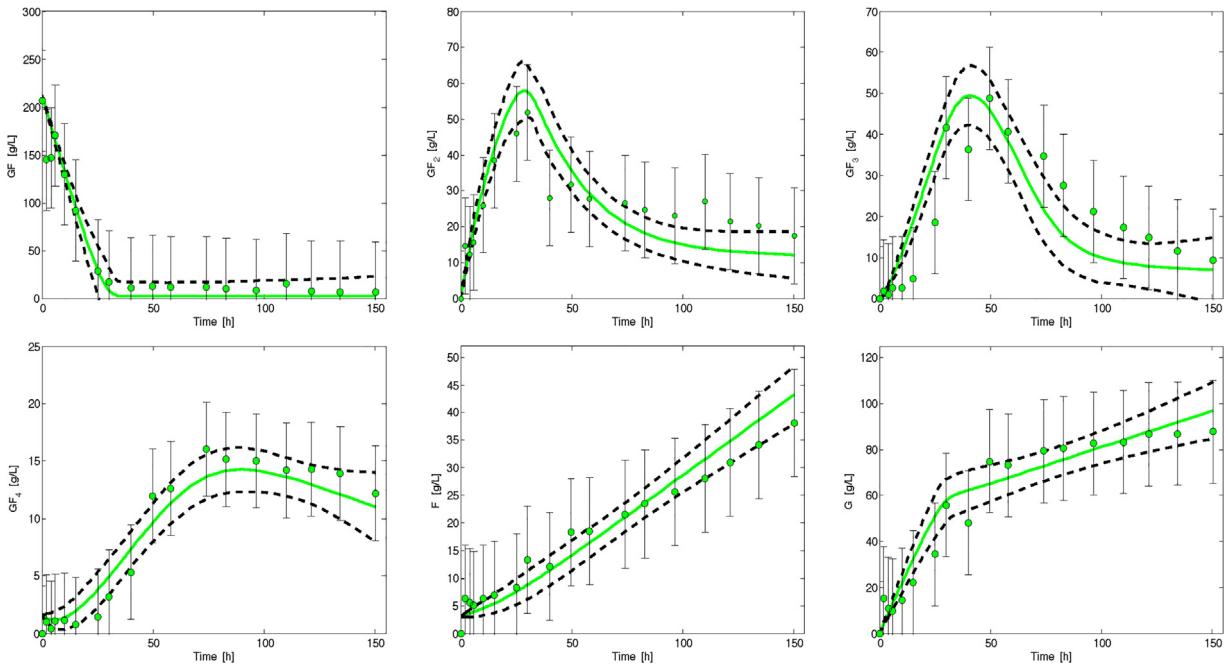

Fig. 9. All the experimental samples of experiment B1 (green dots with black error bars) have a non-empty intersection with the 95%-confidence intervals (dashed lines) of the simulated concentrations (green solid lines).

7.1. Pontryagin maximum principle

The dynamic model can be considered in the form (49), which is affine in the input:

$$\dot{\underline{\xi}}(t) = \underline{f}\left(\underline{\xi}\right) + \sum_{j=1}^{N_u} \underline{g}_j\left(\underline{\xi}\right) u_j(t), \quad \underline{\xi}(t_0) = \underline{\xi}_0\left(\underline{\theta}\right), \quad \text{with } t_0 \le t \le t_f \tag{52}$$

The function $\underline{f}$ represents the dynamics of the chemical process while $\underline{g}$ determines the fed-batch dynamics. t_0 and t_f denote the initial and the final times of the culture. The latter is not known a priori but a final condition on the bioreactor volume is provided by:

$$\Omega = V(t_f) - V_{\max} = 0. \tag{53}$$

where V_{max} is the effective maximal volume.

The objective is to maximize the performance index J defined by

$$J(t_f) = GF_2(t_f) + GF_3(t_f) + GF_4(t_f) \equiv c(\underline{\xi}), \tag{54}$$

which is the sum of the concentration of the FOS at the final time, and is a complex function of the state vector $\underline{\xi}$.

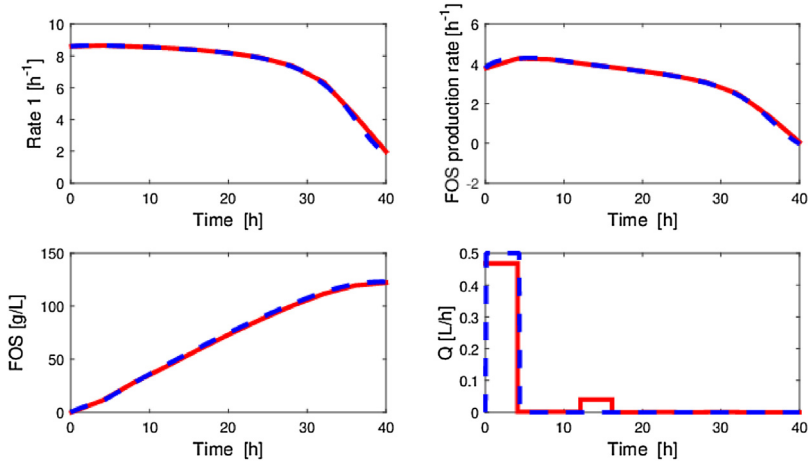

Fig. 10. Optimal (bang-bang) control of FOS production; Comparison of Pontryagin maximum principle and nonlinear programming results. Clockwise from top left – Subplot A: Reaction rate r_1, Subplot B: global FOS production rate, Subplot C: FOS concentration in the broth, Subplot D: optimal substrate feed rate.

The substrate feed rate $u = Q_{in}$ is limited in the range $[Q_{min}\ Q_{\max}]$ by the feed pump characteristics:

$$Q_{\min} \leq Q \leq Q_{\max}. \tag{55}$$

The optimal control consists in finding an admissible control function, $u(t) = Q_{in}(t)$, yielding an admissible trajectory for the system (52), i.e., satisfying (53) and (55), while maximizing the performance index J.

An elegant solution to this problem is provided by the maximum principle of Pontryagin [8]. Maximizing the performance index (54) is equivalent to maximizing the Hamiltonian:

$$H = \phi + \psi \quad u \tag{56}$$

which is affine in the control input, and where the functions ϕ and ψ are given by

$$\phi = \underline{\lambda}^{\top} \underline{f}(\underline{\xi}) \quad \text{and} \quad \psi = \underline{\lambda}^{\top} \underline{g}(\underline{\xi}) \tag{57}$$

The vector $\underline{\lambda}$ is the adjoint or costate vector and has the same dimension as $\underline{\xi}$. It is defined by

$$\frac{d\underline{\lambda}^{\top}}{dt} = -\frac{\partial H}{\partial \underline{\xi}} = -\underline{\lambda}^{\top} \frac{\partial \underline{f}}{\partial \underline{\xi}} - \underline{\lambda}^{\top} \frac{\partial \underline{g}}{\partial \underline{\xi}} u \tag{58}$$

The transversality condition is given by

$$\underline{\lambda}(t_f) = \frac{\partial c(\underline{\xi})}{\partial \underline{\xi}} + \nu \frac{\partial \Omega(\underline{\xi})}{\partial \underline{\xi}} \tag{59}$$

which provide $\lambda_{GF,G,F}(t_f) = 0$, $\lambda_{GF_2,GF_3,GF_4}(t_f) = 1$ and $\lambda_V(t_f) = \nu$ with $\nu \in \mathbb{R}$ where λ_α is the costate associated to the state α.

Thanks to the linear inequality constraints on the control variable, a solution exists in the form of a bang-bang control, possibly with singular arcs. The solution depends on the sign of the partial derivative of the Hamiltonian with respect to u, i.e., the sign of ψ:

$$\begin{cases} \text{if} \quad \psi < 0, \quad \text{then} \quad u = u_{\min}, \\ \text{if} \, \psi = 0, \quad \text{then} \quad u = u_s, \\ \text{if} \, \psi > 0, \quad \text{then} \quad u = u_{\max}. \end{cases} \tag{60}$$

u_s is a singular control law. It is obtained by taking the second time derivative of ψ [8], which yields

$$u_s = -\frac{\underline{\lambda}^{\top} \left(\frac{\partial q}{\partial \underline{\xi}} \underline{f} - \frac{\partial \underline{f}}{\partial \underline{\xi}} \underline{q} \right)}{\underline{\lambda}^{\top} \left(\frac{\partial q}{\partial \underline{\xi}} \underline{g} - \frac{\partial \underline{g}}{\partial \underline{\xi}} \underline{q} \right)} \tag{61}$$

under the condition that $\underline{\lambda}^{\top} \left(\frac{\partial q}{\partial \underline{\xi}} \underline{g} - \frac{\partial \underline{g}}{\partial \underline{\xi}} q \right) \neq 0$, where $\underline{q}$ is defined by

$$\underline{q} = \frac{\partial \underline{g}}{\partial \underline{\xi}} \underline{f} - \frac{\partial \underline{f}}{\partial \underline{\xi}} \underline{g}. \tag{62}$$

Based on this development, a numerical algorithm made of 5 steps can be developed:

1. Guess t_f, ν and a substrate feed rate Q respecting the final condition (53), and integrate forward the model defined by Eq. (52).
2. Determine λ by integrating backward Eq. (58).
3. Integrate forward the model defined in Eq. (52) using bang bang control (60).
4. Repeat Steps 2 and 3, considering $\nu = \nu + \delta\nu$, with $\delta\nu$ as small as required, until $\Omega = 0$.
5. Repeat Steps 2 to 3 with a new guess of t_f in order to maximize the cost function J defined in (54) and push the Hamiltonian (56) to zero.

The final time t_f is increased as long as the obtained FOS concentration profile is monotically increasing. On the other hand, if a maximum is observed, t_f is decreased in order to stop the operation when the maximum is reached.

7.2. Nonlinear programming

A straightforward numerical optimization can also be considered in order to validate the previous approach. For ease of implementation, the problem is slightly reformulated as:

$$\max_{\mathbf{GF_i}(0),\mathbf{Q(t)}} J_{num}(t_f) = GF_2(t_f) + GF_3(t_f) + GF_4(t_f) \tag{63a}$$

$$\text{s.t.} \quad \text{Model}(18) \tag{63b}$$

$$Q_{\min} \leqslant Q(t) \leqslant Q_{\max} \tag{63c}$$

$$V(t) \leqslant V_{\max} \tag{63d}$$

$$V(t_f) = V_{\max} \tag{63e}$$

The optimization is achieved using the nonlinear programming solver *fmincon* of MATLAB, which allows implementing easily the different constraints on Q and V in (63a). The constraints on Q can be considered as simple box constraints on the input. On the other hand, constraints on V are nonlinear, and require the integration of the ODE for the volume in (18) in order to check, at each integration step, the inequality (63d) and, once the state trajectories are

Table 6
Optimal control: constraints and initial conditions.

Hardware constraints		Initial conditions	
GF_{in}	$280\,g\,L^{-1}$	$GF(t_0)$	$200\,g\,L^{-1}$
$Vmax$	3 L	$V(t_0)$	1 L
Q_{max}	$0.5\,L\,h^{-1}$	$G(t_0)$ and $F(t_0)$	$0\,g\,L^{-1}$
Q_{min}	$0\,L\,h^{-1}$	$GF_{2,3,4}(t_0)$	$0\,g\,L^{-1}$

obtained on the time span, equality (63e). The proposed numerical optimization aims at providing a simple solution for comparison purposes. The reader may refer to more advanced algorithms, e.g., the simultaneous approach which can be found in [7].

7.3. Results

The numerical values of the initial conditions and several constraints are listed in Table 6.

For both optimization methods, the evolution of the optimal substrate feed rate is similar (see Fig. 10) and, interestingly, the same final times are obtained: 40 h. Following Pontryagin's method, the maximum feed rate $u = Q_{max} = 0.5\,L\,h^{-1}$ is applied until the bioreactor is filled up, at $t = 4.3$ h, while the nonlinear programming method leads to a constant feed rate of $u = Q = 0.47\,L\,h^{-1}$ during 4.1 h. After these fed-batch phases at high feed rate, Pontryagin's method switches to a batch mode, with no inlet $u = Q_{min} = 0\,L\,h^{-1}$, until the end of the culture. On the other hand, numerical optimization still operates in fed-batch mode at very slow feed rates, i.e., $0.002\,L\,h^{-1}$ until 12 h followed by $0.04\,L\,h^{-1}$ until 16 h where the fed-batch phase definitely ends (the bioreactor is completely filled).

These control moves allow to maximize the production rate of GF_2 which is directly linked to the concentration of GF. This phenomenon is shown through the evolution of the reaction rate r_1 in Fig. 10, which is close to the maximum rate μ_1^{max} (a larger inlet substrate concentration GF_{in} would be required to get even closer). The global FOS production rate, defined by $f_{GF_2} + f_{GF_3} + f_{GF_4}$, keeps increasing during the main fed batch period and reaches its maximum after 4.3 h (see Fig. 10).

A FOS concentration of $123\,g\,L^{-1}$ is obtained after 40 h using Pontryagin's method and $122\,g\,L^{-1}$ using the nonlinear programming method. The productivities and the yields (defined by Eq. (64)) are respectively for Pontryagin's method and nonlinear programming, $\mathcal{P}(t_f) = 3.075\,g\,L^{-1}\,h^{-1}$ and $3.05\,g\,L^{-1}\,h^{-1}$, and $\mathcal{Y}(t_f) = 48.55\%$ and 48.16%.

$$\begin{cases} \mathcal{P}(t_f) = \dfrac{GF_2(t_f) + GF_3(t_f) + GF_4(t_f)}{t_f}, \\ \mathcal{Y}(t_f) = V_{max}\dfrac{GF_2(t_f) + GF_3(t_f) + GF_4(t_f)}{GF(t_0)V(t_0) + GF_{in}(V_{max} - V(t_0))}. \end{cases} \tag{64}$$

8. Conclusion

The main contribution of this study is the derivation of a low-dimension dynamic model of batch and fed-batch cultures of *Aureobasidium pullulans* for the production of Fructo-Oligosaccharides. To the best of our knowledge, it is the first model of this kind with a thorough analysis of the model properties and validation with experimental data. The second contribution is the application of a data-driven procedure combining maximum likelihood principal component analysis, and nonlinear parameter estimation (including the computation of confidence intervals), to derive the model candidates from experimental data. In a systematic way, the models can be derived and possibly simplified, based on a sound analysis of the parameter uncertainties. This procedure is general and can be applied to other bioprocesses, for which prior knowledge is insufficient to develop a first-principle model in a straightforward way. The interested reader is referred to [11] for an application to the cultures of hybridoma cells in sequential fed-batch cultures. The low-dimension model has enough predictive capability to be exploited for dynamic optimization, which is the third contribution of this study. Using Pontryagin maximum principle, an optimal substrate feed rate in the form of a bang-bang control is obtained. First, the bioreactor operates at maximum feed rate. When full, the bioreactor turns to batch mode. In the considered application, a FOS concentration of $123\,g\,L^{-1}$ for a culture time of 40 h is obtained. The resulting operation mode is extremely simple and easy to implement in practice.

Conflicts of interest

The authors declare no conflicts of interest.

Acknowledgments

The authors thank the financial support of F.R.S.-FNRS, the Belgium National Fund for the Scientific Research (Research Project 24643.08).

References

[1] M.B. Alvarado-Huallanco, F. Maugeri-Filho, Kinetics and modeling of fructooligosaccharide synthesis by immobilized fructosyltransferase from *Rhodotorula sp*, J. Chem. Technol. Biotechnol. 85 (2010) 1654–1662.
[2] B. Iooss, P. Lemaître, A review on global sensitivity analysis methods, in: G. Dellino, C. Meloni (Eds.), Uncertainty Management in Simulation-Optimization of Complex Systems. Operations Research/Computer Science Interfaces, 59, Springer, Boston, MA, 2015.
[3] E. Balsa-Canto, A.A. Alonso, J.R. Banga, An iterative identification procedure for dynamic modeling of biochemical networks, BMC Syst. Biol. 4 (2010) 1–18.
[4] G. Bastin, D. Dochain, On-line estimation and adaptive control of bioreactors Process Measurement and Control, vol. 1, Elsevier, Amsterdam, 1990.
[5] G. Bellu, M.P. Saccomani, S. Audoly, L. D'Angiï1/2, Daisy: a new software tool to test global identifiability of biological and physiological systems, Comput. Methods Programs Biomed. 88 (1) (2007) 52–61.
[6] O. Bernard, G. Bastin, On the estimation of the pseudo stoichiometric matrix for macroscopic mass balance modelling of biotechnological processes, Math. Biosci. 193 (2005) 51–77.
[7] L.T. Biegler, An overview of simultaneous strategies for dynamic optimization, Chem. Eng. Process. Process Intensif. 46 (11) (2007) 1043–1053.
[8] A.E. Bryson, H. Yu-Chi, Applied Optimal Control, Ginn and Co., Waltham, Mass, 1969.
[9] O.T. Chis, J.R. Banga, E. Balsa-Canto, Structural identifiability of systems biology models: a critical comparison of methods, PLoS ONE 6 (11) (2011) e27755.
[10] O.T. Chis, J.R. Banga, E. Balsa-Canto, Genssi: a software toolbox for structural identifiability analysis of biological models, Bioinformatics 27 (18) (2011) 2610–2611.
[11] L. Dewasme, F. Côte, P. Filee, A.-L. Hantson, A. Vande Wouwe, Macroscopic dynamic modeling of sequential batch cultures of hybridoma cells: an experimental validation, Bioengineering 4 (1) (2017).
[12] A. Dominguez, C. Nobre, L.R. Rodrigues, A.M. Peres, D. Torres, I. Rocha, New improved method for fructooligosaccharides production by *Aureobasidium pullulans*, Carbohydr. Polym. 89 (2012) 1174–1179.
[13] K.J. Duan, J.S. Chen, D.C. Sheu, Kinetic studies and mathematical model for enzymatic production of fructooligosaccharides from sucrose, Enzyme Microb. Technol. (1994) 334–339.
[14] K.J. Duan, J.S. Chen, D.C. Sheu, Kinetic studies and mathematical model for enzymatic production of fructooligosaccharides from sucrose, Enzyme Microb. Technol. 16 (1994) 334–339.
[15] R. Fekih-Salem, A. Vande Wouwer, C. De Castro, C. Nobre, A.-L. Hantson, Parameter identification of the fermentative production of fructo-oligosaccharides by *Aureobasidium pullulans*, Proceedings of the 19th International Conference on System Theory, Control Computing (2015) 43–48.
[16] A. Fiordalis, C. Georgakis, Data-driven, using design of dynamic experiments, versus model-driven optimization of batch crystallization processes, J. Process Control 23 (2) (2013) 179–188.
[17] F. Guio, L.D. Rugeles, S.E. Rojas, M.P. Palomino, M.C. Camargo, O.F. Sï1/2nchez, Kinetic modeling of fructooligosaccharide production using *Aspergillus oryzae N74*, Appl. Biochem. Biotechnol. 167 (2012) 142–163.
[18] K.U. Jung, J.W. Run, K.R. Kang, J.Y. Lim, J.H. Lee, Mathematical model for enzymatic production of fructo-oligosaccharides from sucrose, Enzyme Microb. Technol. 11 (1989) 491–494.
[19] J. Karlsson, M. Anguelova, M. Jirstrand, An efficient method for structural identiability analysis of large dynamic systems, Proceedings of the 16th IFAC Symposium on System Identification, vol. 16 (2012) 941–946.

[20] A. Kiparissides, C. Georgakis, A. Mantalaris, E.N. Pistikopoulos, Design of in silico experiments as a tool for nonlinear sensitivity analysis of knowledge-driven models, Ind. Eng. Chem. Res. 53 (1) (2014) 7517–7525.
[21] J. Mailier, M. Remy, A. Vande Wouwer, Stoichiometric identification with maximum likelihood principal component analysis, J. Math. Biol. 67 (2013) 739–765.
[22] K.A.P. McLean, K.B. McAuley, Mathematical modelling of chemical processes-obtaining the best model predictions and parameter estimates using identifiability and estimability procedures, Can. J. Chem. Eng. 90 (2) (2012) 351–366.
[23] T. Mutanda, M.P. Mokoena, A.O. Olaniran, B.S. Wilhelmi, C.G. Whiteley, Microbial enzymatic production and applications of short-chain fructooligosaccharides and inulooligosaccharides: recent advances and current perspectives, J. Ind. Microbiol. Biotechnol. 41 (6) (2014) 893–906.
[24] K. Nishizawa, M. Nakajima, H. Nabetani, Kinetic study on transfructosylation by b-fructofuranosidase from *Aspergillus niger ATCC 20611* and availability of a membrane reactor for fructooligosaccharide production, Food Sci. Technol. Res. 7 (1) (2001) 39–44.
[25] C. Nobre, M.J. Santos, A. Dominguez, D. Torres, O. Rocha, A.M. Peres, I. Rocha, E.C. Ferreira, J.A. Teixeira, L.R. Rodrigues, Comparison of adsorption equilibrium of fructose, glucose and sucrose on potassium gel-type and macroporous sodium ion-exchange resins, Anal. Chim. Acta 654 (1) (2009) 71–76.
[26] K. Pearson, On lines and planes of closest fit to systems of points in space, Philos. Mag. 2 (6) (1901) 559–572.
[27] H. Pohjanpalo, System identifiability based on the power series expansion of the solution, Math. Biosci. 4 (1–2) (1978) 21–33.
[28] C.R. Rao, Information and the Accuracy Attainable in the Estimation of Statistical Parameters, vol. 37, Bulletin of the Calcutta Mathematical Society, Kolkata, India, 1945, pp. 81–89.
[29] J.F. Ritt, Differential Algebra, American Mathematical Society, Providence, Rhode Island, 1950.
[30] O. Rocha, C. Nobre, A. Dominguez, D. Torres, N. Faria, L. Rodrigues, J.A. Teixeira, E.C. Ferreira, I. Rocha, A dynamical model for the fermentative production of fructooligosaccharides, 10th International Symposium on process systems engineering (2009) 1–7.
[31] P.T. Sangeetha, M.N. Ramesh, S.G. Prapulla, Recent trends in the microbial production, analysis and application of fructooligosaccharides, Trends Food Sci. Technol. 16 (2005) 442–457.
[32] J. Schorsch, M. Kinnaert, R. Fekih-Salem, L. Dewasme, C.C. Castro, A. Vande Wouwer, Identification and optimal control of fructo-oligosaccharide production, Proc. 10th IFAC International Symposium on Advanced Control of Chemical Processes (ADCHEM) (2018) 672–677.
[33] M. Simeone, I.B. Hogue, C.J. Ray, D.E. Kirschner, A methodology for performing global uncertainty and sensitivity analysis in systems biology, J. Theor. Biol. 254 (1) (2008) 178–196.
[34] I.Y. Smets, J.E. Claes, E.J. November, G.P. Bastin, J.F. Van Impe, Optimal adaptive control of (bio)chemical reactors: past, present and future, J. Process Control 14 (2004) 795–805.
[35] J.F. Van Impe, G. Bastin, Optimal adaptative control of fed-batch fermentation processes, Control Eng. Pract. 3 (7) (1995) 939–954.
[36] A.F. Villaverde, A. Barreiro, Identifiability of large nonlinear biochemical networks, MATCH Commun. Math. Comput. Chem. 76 (2016) 259–296.
[37] E. Walter, Y. Lecourtier, Global approaches to identifiability testing for linear and nonlinear state space models, Math. Comput. Simul. 24 (1982) 472–482.
[38] E. Walter, L. Pronzato, Identification of parametric models from experimental data, in: Communications and Control Engineering, Springer-Verlag, Berlin, 1997.
[39] P.D. Wentzell, D.T. Andrews, D.C. Hamilton, K. Faber, B.R. Kowalski, Maximum likelihood principal component analysis, J. Chemom. 11 (1997) 339–366.
[40] H. Yue, M. Brown, J. Knowles, H. Wang, D.S. Broomhead, D.B. Kellab, Insights into the behaviour of systems biology models from dynamic sensitivity and identifiability analysis: a case study of an nf-kappab signalling pathway, Mol. Biosyst. 12 (2006).
[41] J.W. Yun, S.K. Song, The production of high-content fructo-oligosaccharides from sucrose by the mixed-enzyme system of fructosyltransferase and glucose-oxidase, Biotechnol. Lett. 15 (1993) 573–576.